CSIRO PUBLISHING

International Journal of Wildland Fire **2018**, *27*, 217–227
https://doi.org/10.1071/WF17069

Estimating the area burned by agricultural fires from Landsat 8 Data using the Vegetation Difference Index and Burn Scar Index

Shudong Wang[A], *Muhammad Hasan Ali Baig*[B], *Suhong Liu*[C], *Huawei Wan*[D], *Taixia Wu*[D,F] *and Yingying Yang*[E]

[A]Institute of Remote Sensing and Digital Earth, Chinese Academy of Sciences, Beijing 100101, China.
[B]Institute of Geo-Information and Earth Observation (IGEO), Pir Mehr Ali Shah Arid Agriculture University, Rawalpindi, 46300, Pakistan.
[C]School of Geography, Beijing Normal University, Beijing 100875, China.
[D]Satellite Environment Centre, Ministry of Environmental Protection, Beijing 100094, China.
[E]School of Earth Sciences and Engineering, Hohai University, Nanjing, 211100, China.
[F]Corresponding author. Email: wutx@hhu.edu.cn

Abstract. Obtaining an accurate estimate of the area of burned crops through remote sensing provides extremely useful data for the assessment of fire-induced trace gas emissions and grain loss in agricultural areas. A new method, incorporating the Vegetation Difference Index (VDI) and Burn Scar Index (BSI) models, is proposed for the extraction of burned crops area. The VDI model can greatly reduce the confounding effect of background information pertaining to green vegetation (forests and grasslands), water bodies and buildings; subsequent use of the BSI model could improve the accuracy of burned area estimations because of the reduction in the influence of background information. The combination of VDI and BSI enables the VDI to reduce the effect of non-farmland information, which in turn improves the accuracy and speed of the BSI model. The model parameters were established, and an effects analysis was performed, using a normalized dispersion value simulation based on a comparison of different types of background information. The efficacy of the VDI and BSI models was tested for a winter wheat planting area in the Haihe River Basin in central China. In comparison with other models, it was found that this method could effectively extract burned area information.

Additional keywords: remote sensing of environment.

Received 19 April 2017, accepted 15 February 2018, published online 10 April 2018

Introduction

Farmers worldwide often remove excess crop residue from fields by burning farmland. The economic benefits of crop residue utilisation are not high, and burning is a quick and cheaper management method. Fire can also remove weeds, pests and diseases, enabling farmers to prepare the next crop (McCarty *et al.* 2009). In the early ripening season (mostly early June) in winter wheat planting areas such as the Haihe River Basin in northern China, it is easy for farmers to lose control of fires owing to dry weather, wind and other natural factors. This can result in the loss of unharvested crops. Frequent farmland fires have serious consequences, such as fire-induced trace gas emissions (Andreae and Crutzen 1997; Andreae and Merlet 2001; Yang *et al.* 2008; Hao and Larkin 2014) and grain loss. Farmland fires that spread to neighbouring grasslands and forests are also one of the main causes of wildland fires (Houghton *et al.* 2000). Some of these fires are caused by stubble and straw burning, whereas others involve the burning of mature crops and are made worse by dry conditions (Maingi and Henry 2007; Vadrevu and Lasko 2015). Because of the randomness and rapid spread of fires on farmland such as the winter wheat planting area in the Haihe River Basin, fire managers find it difficult to determine the location of fires and measure the extent of burned area. Retrieval of accurate burned area data is essential for determining the source of wildland fire, and modelling air pollution and grain loss (França *et al.* 2014).

Most previous studies estimating burned area through remote sensing have classified images using principal component analysis and vegetation indices (Carlson and Ripley 1997; Chuvieco *et al.* 2002; Domenikiotis *et al.* 2002; Hudak and Brockett 2004; Mitri and Gitas 2004; Kučera *et al.* 2005; Loboda *et al.* 2007; Maingi and Henry 2007; Smith *et al.* 2007; Chuvieco *et al.* 2008; Palandjian *et al.* 2009; Stroppiana *et al.* 2009; Boschetti *et al.* 2010; Bastarrika *et al.* 2011; Parker *et al.* 2015). Many studies have relied on the Normalized Difference Vegetation Index (NDVI), including modified versions to reduce the sensitivity of the index to different atmospheric and soil conditions (Chuvieco *et al.* 2002; Domenikiotis *et al.* 2002; Kučera *et al.* 2005; Stroppiana *et al.* 2009; Veraverbeke *et al.* 2011*a*). Some of these modified NDVI indices, such as the Enhanced Vegetation Index (EVI), Soil Adjusted Vegetation Index (SAVI) and Modified Soil-Adjusted Vegetation Index (MSAVI), have been used effectively for burned area estimation in a range of habitats such as forests and grasslands (Huete 1988; Pinty and Verstraete 1992; Qi *et al.* 1994; Huete *et al.* 2002). Some researchers have also proposed other spectral indices, such as the Burned Area Index (BAI) and Normalized Burned Ratio (NBR) (Chuvieco *et al.* 2002; French *et al.* 2008; Veraverbeke *et al.* 2010*b*; Araújo and Ferreira 2015), which are particularly sensitive to the spectral features of a burned area. However, the existence of different land types can easily lead to spectral confusion for burned areas and spectrally similar areas, such as water bodies, roads and buildings, which results in uncertainties in burn scar models, largely due to the difficulty in determining threshold values for these models (Lasaponara 2006; Stroppiana *et al.* 2009; Boschetti *et al.* 2010; Veraverbeke *et al.* 2011*a*, 2011*b*; Boschetti *et al.* 2015). To deal with this type of spectral complexity (spectral mixing), various models and methods have been used to highlight fire-induced changes in pre- and post-fire imagery; however, this can potentially create additional constraints in relation to image-to-image normalisation (Conghe Song and Woodcock 2003; Verbyla *et al.* 2008; Veraverbeke *et al.* 2010*a*, 2010*b*, 2011*a*, 2011*b*).

A few remote sensing methods have been used to extract burn scar information, with a focus mainly on forests, grasslands and other non-farmland land types. Only a few models and methods have addressed the issue of identifying burned areas within farmland. Cultivated land is often distributed unevenly and characterised by a mixture of different land-use types, such as rural settlements, mines, water conservation and irrigation facilities, rivers, lakes and asphalt roads. As a result, different land types often share the same spectra, which creates interference when burn scar information is extracted from remote sensing data. In addition, because of differences in crop types and planting times, the distribution of crop stubble, as well as the presence of mature and non-mature crops, is likely to cause interference, leading to uncertainty in estimations of burned crop area.

The main purpose of the present study was to develop a method for effectively extracting information on the burned crop area caused by agricultural fires from remotely sensed data. Considerable spectral confusion exists in relation to distinguishing burned areas from areas with similar surface features in monotemporal imagery (Lasaponara 2006; Stroppiana *et al.* 2009; Veraverbeke *et al.* 2011*b*). The following issues are of considerable importance regarding the extraction of precise information on burned areas: (1) the method should allow rapid identification of the spatial distribution of mature crops in such a way that researchers can determine the possible range of a burned area, and can reduce the complexity of background information; (2) furthermore, the method can clearly highlight burned areas and integrate different types of background information, for example on mature crops and stubble.

To test the accuracy of the proposed method in determining the locations of burned areas, we selected the winter wheat planting area in the Haihe River Basin. The growth curve features extrapolated from a time series of Moderate Resolution Imaging Spectroradiometer (MODIS) data; based on this, two NDVI images extracted from Landsat 8 data were selected for this area. Burned areas with different spectral features, based on the band features of Landsat 8 data, were analysed and a burn scar index (BSI) was then constructed for extracting information on the burned area. Model application and validation were conducted for the winter wheat planting area of the Haihe River Basin. The method greatly improved the accuracy of satellite image-based burn scar estimates of burnt areas resulting from farmland fires. It can also be used to determine the local and regional contributions of particulate and trace gas emissions, which affect both air quality and public health (McCarty *et al.* 2009; Li *et al.* 2014; Chen *et al.* 2017).

Study area, data collection and data processing

Study area

The Haihe River Basin, China's major grain production base, is located in central China, and covers a total area of 318 200 km^2. The study area is located west of the Haihe River Basin and the main grain crops include winter wheat and maize, as shown in Fig. 1. The mean annual temperature in the study area ranges from 12.7 to 13.7°C, whereas the mean annual precipitation is about 600 mm, based on data from the Anyang Meteorological Bureau. Only sparse precipitation occurs during spring and the air is generally dry; therefore, winter wheat normally requires irrigation. After the winter wheat reaches maturity or is

Fig. 1. Location of the Haihe River Basin, China. The study area is located to the south of the Haihe River Basin and is shown by the red box.

harvested, prescribed fires or wildfires in farmland areas may cause serious air pollution and a loss of grain harvesting opportunities. On 9 June 2015, an agricultural wildfire disaster resulted in the loss of many human lives and large amounts of grain in the study area.

Data collection

Soil, winter wheat and burned area spectral data were collected through field experiments during winter wheat growth and maturity periods. Winter wheat spectral data were collected from 4 April to 3 June in both 2001 and 2002, and stubble and burn spectral data were collected from 9 to 14 June 2015.

An ASD FieldSpec3 spectrometer (Analytical Spectral Devices, Boulder, CO, USA) and a PSR spectrometer (Spectral Evolution Co., Lawrence, MA, USA) were used for field data collection. These devices have a bandwidth between 350 and 2500 nm, a viewing angle of 25° and a height of 20 cm to the measured sample. Measurements were conducted on sunny days with favourable visibility according to the criterion of 3 days in a row without precipitation prior to spectral measurement. The areas surrounding the measurement points were broad, with no large obstructions, and the measurements were conducted at the local time of 1000–1400 hours. Each sample was measured 10 times, and the average reflectance of each sample was then calculated. The total collected sample number was 212. Portions of the spectrum near 1900 nm were removed because of noise.

Data processing

A time series of MODIS 09A data products was selected for crop growth curve analysis. Landsat 8 reflectance data were used for the vegetation difference index (VDI) and BSI models, and Gaofen-1 satellite (GF-1) (Jia *et al.* 2016) data were used for model validation (Table 1). A topographic map with a scale of 1 : 100 000, and some latitude and longitude coordinates, were derived from a Google Earth map of the study area, enabling geometric rectification to be conducted.

ENVI software (ver. 4.8; ITT Visual Solutions, Boulder, CO, USA) was used for spatial geometric precision correction. The correction was accurate to within half a pixel, which enabled transformation of the data into a universal transverse Mercator (UTM) projection.

Method and model

All analyses of the burned area estimates for the study region were conducted using *ENVI* software (ver. 4.8). Fig. 2 is a flowchart of the steps implemented to satisfy the study objectives. The methodology can be divided into four parts: (i) deriving a crop phenology curve from a time series of MODIS NDVI data, which is used to select the date of the TM image. The reference TM image was obtained during the vigorous growth period of the winter wheat; the monitored TM image was obtained just after the fire; (ii) development of a burned area extraction method based on VDI and BSI; (iii) cross-comparison with the results from a previous model (Table 2); and (iv) burned area simulation using VDI and BSI.

Spectral analysis of the typical underlying surfaces in the study area

Ground spectral measurements of the typical underlying surfaces in the study area were conducted using a portable ground object spectrometer (Model PSR-3500m Spectral Evolution Co.), with the spectrum ranging from 400 to 2500 nm (Figs 3 and 4). Moisture absorption bands at 1360–1420 and 1780–1986 nm were removed from the curves.

As shown in Fig. 4, the winter wheat reflectance spectrum for the filling stage peaked at 530 and 1610 nm, with absorption troughs at 680 and 1420 nm and a high reflection region between 760 and 1300 nm. The trend in the variation of the spectrum for mature winter wheat was similar to that of green winter wheat, although the reflection peaks and absorption valleys were more obvious in the former. The reflection peaks and absorption troughs of mature winter wheat in the infrared region (760–1100 nm) were lower than those at the filling stage, whereas in the other bands, they were higher.

The trend in the variation of the burned area spectrum was similar to that of the stubble and soil spectra throughout the

Table 1. Sources for the remote sensing data employed in the present study

Abbreviations: MODIS, Moderate Resolution Imaging Spectroradiometer; GF-1, Gaofen-1 satellite; NIR, near-infrared; SWIR, short-wave infrared

Satellite data	Acquisition time	Path and row	Spatial resolution (m)	Spectral resolution (μm)	Product grade	Source
MODIS	1 January to 28 December 2014	h27v05	250	0.62–1.4385 (36 bands)	MOD09Q1	http://www.gscloud.cn/ (20 March 2018)
Landsat8	2 May to 10 June 2015	124/05	30	Coastal (0.433–0.453) Blue (0.450–0.515) Green (0.525–0.600) Red (0.630–0.680) NIR (0.845–0.885) SWIR 1 (1.560–1.660) SWIR 2 (2.100–2.300) Cirrus (1.360–1.390)	Reflectance	http://earthexplorer.usgs.gov/ (20 March 2018)
GF-1	11 June 2015	856/519	2 (pan)	0.45–0.52 0.52–0.59	L1A	http://www.cresda.com/EN/satellite/7155.shtml (20 March 2018)
		856/520	8 (multispectral)	0.63–0.69 0.77–0.89		

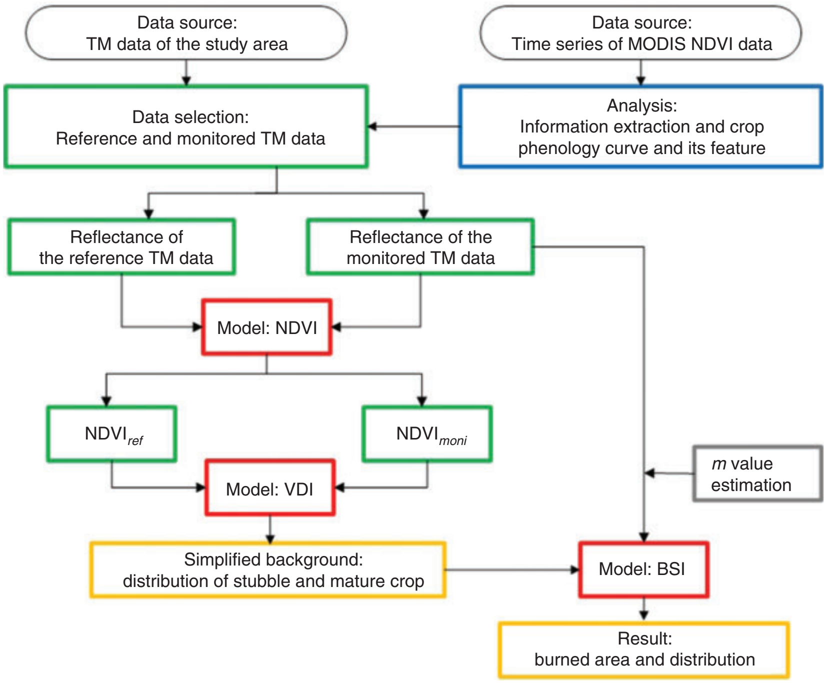

Fig. 2. Overview of the methodology implemented in this study. Abbreviations: BSI, Burn Scar Index; VDI, Vegetation Difference Index; MODIS, Moderate Resolution Imaging Spectroradiometer; NDVI$_{ref}$, Normalized Difference Vegetation Index of the reference remote sensing image; NDVI$_{moni}$, Normalized Difference Vegetation Index of the monitored remote sensing image.

Table 2. Spectral indices used in this study

Abbreviations: R, red; NIR, near-infrared; SWIR, short-wave infrared; LSWIR, longer short-wave infrared; *L*, adjusted parameter

Model	Abbreviation	Formula	Reference
Soil Adjusted Vegetation Index	SAVI	$\mathrm{SAVI} = (1 + L)\dfrac{\mathrm{NIR} - R}{\mathrm{NIR} + R + L}$ with $L = 0.5$	Huete 1988
Burned Area Index	BAI	$\mathrm{BAI} = \dfrac{1}{(0.1 + R)^2 + (0.06 + NIR)^2}$	Chuvieco *et al.* 2002
Normalized Burn Ratio	NBR	$\mathrm{NBR} = \dfrac{\mathrm{NIR} - \mathrm{LSWIR}}{\mathrm{NIR} + \mathrm{LSWIR}}$	Key and Benson 2006
Char Soil Index	CSI	$\mathrm{CSI} = \dfrac{\mathrm{NIR}}{\mathrm{SWIR}}$	Smith *et al.* 2007
Mid-Infrared Burn Index	MIRBI	$\mathrm{MIRBI} = 10\mathrm{LMIR} - 9.8\mathrm{SMIR} + 2$	Trigg and Flasse 2001

entire spectral range. The reflectance of the burned area was generally weak in the 400–1800-nm band range, while it was higher than that of mature winter wheat and the filling stage at 1800–2500 nm. The curve in the 1800–2500-nm region was similar to those of soil and stubble. This result was similar to that reported in previous studies (Lasaponara 2006; Smith *et al.* 2007; Chuvieco *et al.* 2008). The purpose of the ground spectral measurements was to obtain the features of different underlying surfaces and then use them to select bands from Thematic Mapper (TM) images. For certain features, the second to seventh TM bands overlapped the spectrum curves measured by the spectrometer, as shown by the short horizontal lines in Fig. 4.

Time series of the NDVI analysis

For the VDI parameters NDVI$_{ref}$ and NDVI$_{moni}$, NDVI$_{ref}$ in the subtrahend represents the NDVI value during the growth period, and NDVI$_{moni}$ represents the NDVI value during the mature period. An analysis of the NDVI curves for different growth stages of the typical underlying surfaces was conducted in the Haihe River Basin (Fig. 5). The NDVI curve from the time series of the MODIS data was used to analyse trends in the NDVI with respect to differences between crop area and other typical underlying surfaces, such as forests and grasslands, and cities and towns. The time series of NDVI values for winter wheat began to increase from Julian day 40 and peaked between Julian

Fig. 3. Photographs of mature winter wheat (*a*), stubble (*b*) and burned areas (*c*) within the study area.

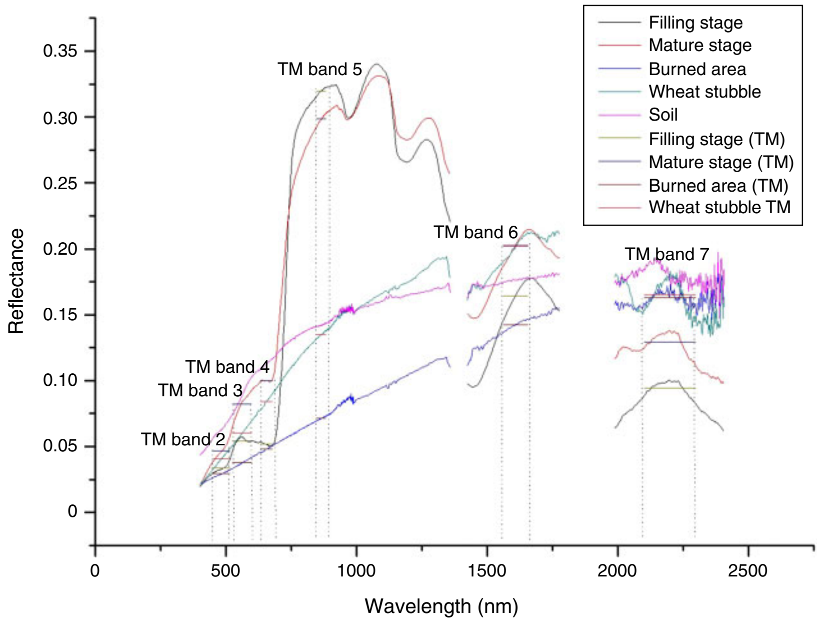

Fig. 4. Spectrum curves of the typical underlying surfaces in the study area overlapped with Thematic Mapper (TM) bands. The continuous spectrum curves were measured using a spectrometer, and the short horizontal lines are the second to seventh TM bands of the corresponding underlying surfaces.

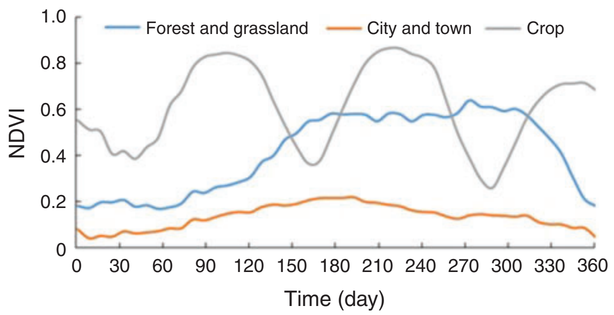

Fig. 5. Changes in wheat phenology over 1 year obtained from MODIS time series data.

days 90 and 120, when the curve began to decline, reaching its lowest value at approximately Julian day 170 (Fig. 5).

In comparison with the NDVI curves of forests and grasslands, and of cities and towns, the NDVI curves of the winter wheat were higher before Julian day 140, but declined before Julian day 170. From the above analysis, it is clear that the NDVI curve of winter wheat changed over time, and was also different from that of forests and grasslands as well as cities and towns.

The models and their parameters

The VDI model

Based on the above time series of NDVI curve analysis, a VDI was developed, and specific models and parameters were configured as below:

$$\mathrm{VDI} = \mathrm{NDVI}_{ref} - \mathrm{NDVI}_{moni}, \tag{1}$$

where the NDVI is given by $(R_{\mathrm{Nir}} - R_{\mathrm{Red}})/(R_{\mathrm{Nir}} + R_{\mathrm{Red}})$. R_{Nir} and R_{Red} are the fifth (near-infrared (NIR)) and fourth (red) bands of the Landsat 8 sensor respectively. NDVI_{ref} in the equation represents the NDVI value during the growth period and NDVI_{moni} represents the NDVI value during the mature period.

The BSI model and its parameters

Previous observations and analyses (Veraverbeke *et al.* 2011*a*) demonstrated a low discriminatory power for the visible spectral region, and indicated that the highest sensitivity is in the short-wave infrared (SWIR) spectral region.

The specific parameters of the BSI are described below. Background features such as soil, stubble and mature crop, can be defined as:

$$\mathrm{BSI} = \frac{(R_{\mathrm{SW}} - R_{\mathrm{Red}})}{(R_{\mathrm{SW}} + R_{\mathrm{Red}})\left(R^m_{\mathrm{Green}} + R^m_{\mathrm{Red}} + R^m_{\mathrm{Nir}}\right)}, \quad (2)$$

where R_{SW}, R_{Red}, R_{Nir}, and R_{Green} are Landsat 8 bands 7 (SWIR 2), 4 (red), 5 (NIR) and 3 (green) respectively. The equation $(R_{\mathrm{SW}} - R_{\mathrm{Red}})/(R_{\mathrm{SW}} + R_{\mathrm{Red}})$ is proposed based on spectral analysis of the relationship between the burned area and the background information. The R_{SW} value of a burned area is similar to those of soil and stubble, and is higher than that of a mature crop. However, the R_{Red} value of a burned area is lower than those of soil, stubble and mature winter wheat. In the denominator, *m* is an adjustment factor. An appropriate value of *m* for $\left(R^m_{\mathrm{Green}} + R^m_{\mathrm{Red}} + R^m_{\mathrm{Nir}}\right)$ can highlight burned areas, reduce the influence of background information, and reduce differences between the different types of background information (thereby reducing uncertainty in the estimation of burned areas). A value of 4 for *m* was considered appropriate for the present study according to the simulation analysis (Tables 3 and 4).

Table 3. Comparison of Burn Scar Index (BSI) values of typical underlying surfaces and C() values for different *m* values(the bold number is the biggest C() value of each *m* value)
See text for definition of terms

C	BSI-0 ($m=0$)	BSI-2 ($m=2$)	BSI-4 ($m=4$)	BSI-6 ($m=6$)
$\overline{S}\,\overline{B}$	0.155	3.172	154.127	6462.467
$\overline{S}\,\overline{B}$	0.269	5.422	259.517	10976.981
$\overline{S}$	0.095	0.873	16.089	245.779
$\overline{M}$	0.229	1.367	17.601	191.191
C(*SB* vs *S*)	0.06	2.299	138.038	6216.688
C(*SB* vs *M*)	−0.074	1.805	136.526	6271.276
C(*MB* vs *S*)	**0.174**	**4.549**	**243.46**	10731.2
C(*MB* vs *M*)	0.04	4.055	241.948	**10785.79**

Table 4. Comparison of the Burn Scar Index (BSI) values of typical underlying features and *ND*() (normalized *C*()) values for different values of *m*
See text for definition of terms

($/C_{\max}$)	BSI-0 /0.174	BSI-2 /4.549	BSI-4 /243.46	BSI-6 /10785.79
ND(*SB* vs *S*)	0.3448	0.5054	0.5670	0.5764
ND(*SB* vs *M*)	−0.425	0.3968	0.5608	0.5814
ND(*MB* vs *S*)	1	1.000	1	0.9950
ND(*MB* vs *M*)	0.2299	0.8914	0.9938	1

C denotes comparison between various types of background information and the information valuable for the BSI.

$$C(SB\,\mathrm{vs}\,S) = \left|\overline{S} - \overline{S}\,\overline{B}\right|, \quad (3)$$

$$C(MB\,\mathrm{vs}\,S) = \left|\overline{S} - \overline{M}\,\overline{B}\right|, \quad (4)$$

$$C(MB\,\mathrm{vs}\,S) = \left|\overline{S} - \overline{M}\,\overline{B}\right|, \quad (5)$$

$$C(MB\,\mathrm{vs}\,M) = \left|\overline{M} - \overline{M}\,\overline{B}\right|, \quad (6)$$

where $\overline{S}\,\overline{B}$ is the mean BSI of the burned stubble area retrieved from a Landsat 8 image, $\overline{M}\,\overline{B}$ is the mean BSI of the burned mature crop area in the same image, $\overline{S}$ is the mean BSI of the unburned stubble area, and $\overline{M}$ is the mean BSI of the unburned mature crop area. C() is the difference between the two compared parameters; the larger the value of C(), the greater the difference between the two compared parameters. The proportions of these different land-cover types within burned and unburned areas were validated by field sampling and high-resolution satellite images (i.e. GF-1 data). Based on the classification results for the Landsat 8 image, the locations of the samples were obtained and the mean value of each cover type was calculated.

To facilitate the analysis, the range of *C*() was normalized to (0,1) (Wang *et al.* 2015). $C_{\max}$ is the maximum value of $C(SB\,\mathrm{vs}\,S)$, $C(SB\,\mathrm{vs}\,M)$, $C(MB\,\mathrm{vs}\,S)$ and $C(MB\,\mathrm{vs}\,M)$, calculated as follows:

$$ND(SB\,\mathrm{vs}\,S) = C(SB\,\mathrm{vs}\,S)/C_{max}, \quad (7)$$

$$ND(SB\,\mathrm{vs}\,M) = C(SB\,\mathrm{vs}\,M)/C_{max}, \quad (8)$$

$$ND(MB\,\mathrm{vs}\,S) = C(MB\,\mathrm{vs}\,S)/C_{max}, \quad (9)$$

$$ND(MB\,\mathrm{vs}\,M) = C(MB\,\mathrm{vs}\,M)/C_{max}, \quad (10)$$

where $ND(SB\,\mathrm{vs}\,S)$, $ND(SB\,\mathrm{vs}\,M)$, $ND(MB\,\mathrm{vs}\,S)$, and $ND(MB\,\mathrm{vs}\,M)$ are the normalized values of $C(SB\,\mathrm{vs}\,S)$, $C(SB\,\mathrm{vs}\,M)$, $C(MB\,\mathrm{vs}\,S)$, and $C(MB\,\mathrm{vs}\,M)$ respectively.

Results and discussion

Estimation of m

By retrieving the values of $\overline{S}\,\overline{B}$, $\overline{M}\,\overline{B}$, $\overline{S}$ and $\overline{M}$ for the study area from a Landsat 8 image, a set of *m* values from 0 to 10 was obtained in increments of 0.5. The *m* values of 0, 2, 4 and 6 were selected and used in example calculations. Then, the BSI and *C*() values were calculated, as shown in Table 3. The maximum values of $C(SB\,\mathrm{vs}\,S)$, $C(SB\,\mathrm{vs}\,M)$, $C(MB\,\mathrm{vs}\,S)$, and $C(MB\,\mathrm{vs}\,M)$ were calculated for different values of *m*. $ND(SB\,\mathrm{vs}\,S)$, $ND(SB\,\mathrm{vs}\,M)$, $ND(MB\,\mathrm{vs}\,S)$, and $ND(MB\,\mathrm{vs}\,M)$ were calculated as shown in Table 4. Fig. 6 shows the four *ND*() curves with *m* values ranging from 0 to 10, in increments of 0.5. An *ND*() value of 1 indicates that the two parameters being compared are totally distinct, whereas the closer the value is to 0, the less distinct are the parameters. In Fig. 6, in a comparison of the different *m* values for the BSI model, each of the four *ND*() curves reaches a saturation value when *m* is close to 4. A BSI model in which $m = 4$ has a high compression capability and can provide detailed background information.

Verification of the VDI and BSI models

Verification of the VDI model

The VDI model was prepared using two NDVI images extracted from Landsat 8 data (Fig. 7) and 950 groups of BSI values were obtained from field samples and high-spatial-resolution GF-1 satellite data. The 2-m-resolution GF-1 remote sensing fusion data were based on the multispectral and panchromatic bands images by using the Nearest Neighbor Decision (NND) fusion method. The overall precision of the model exceeded 95% with respect to estimation of mature winter wheat and stubble areas.

Mature winter wheat data could be extracted with the VDI model by setting a threshold, with the results indicating that an obvious difference between $NDVI_{ref}$ and $NDVI_{moni}$ values allows more effective extraction. Therefore, a large NDVI value as $NDVI_{t0}$ and small NDVI value as $NDVI_t$ should be selected to present a very different trend in the change in forest and grassland and cities and towns, from that in winter wheat cover between Julian days 140 and 170 (Fig. 8).

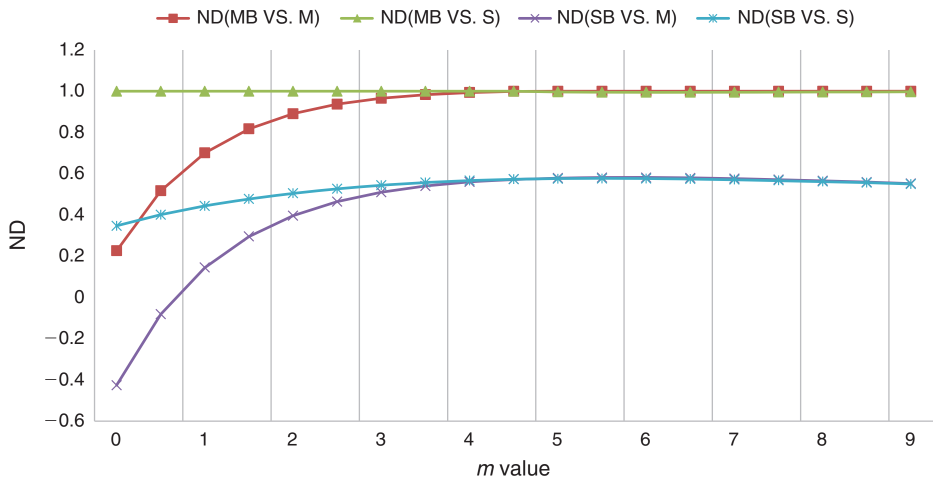

Fig. 6. Comparison of the four types of *ND*() value for the Burn Scar Index (BSI) model according to different values of *m*.

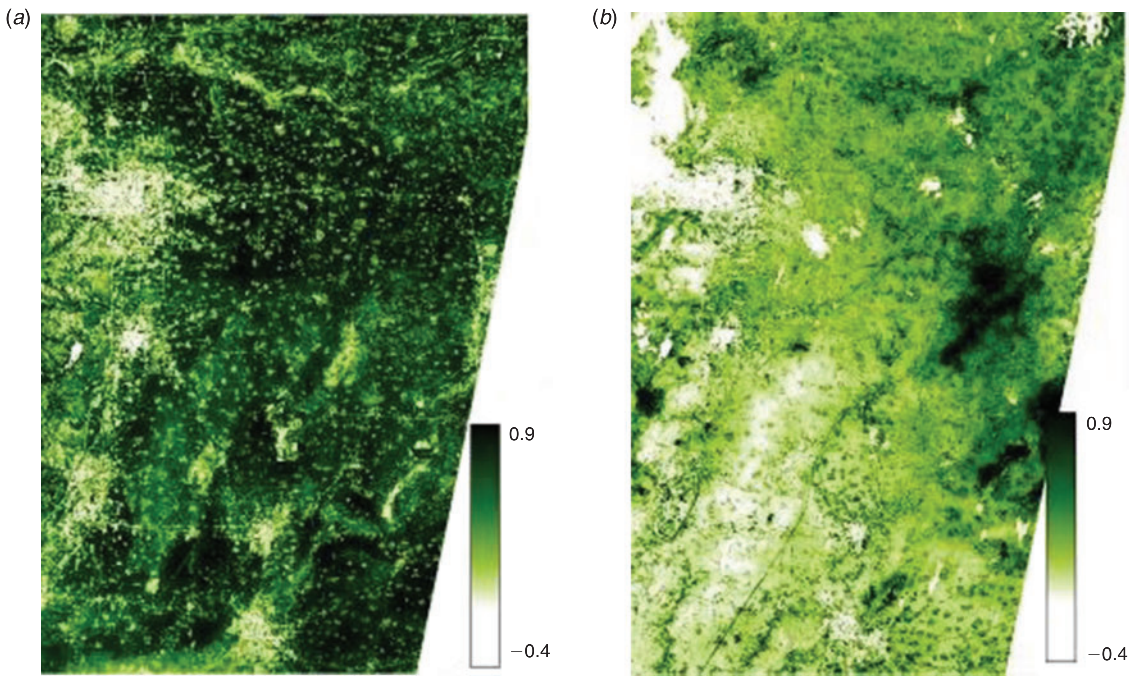

Fig. 7. Normalized Difference Vegetation Index (NDVI) values on Julian days 145 (*a*), and 161 (*b*) using Landsat 8 reflectance data.

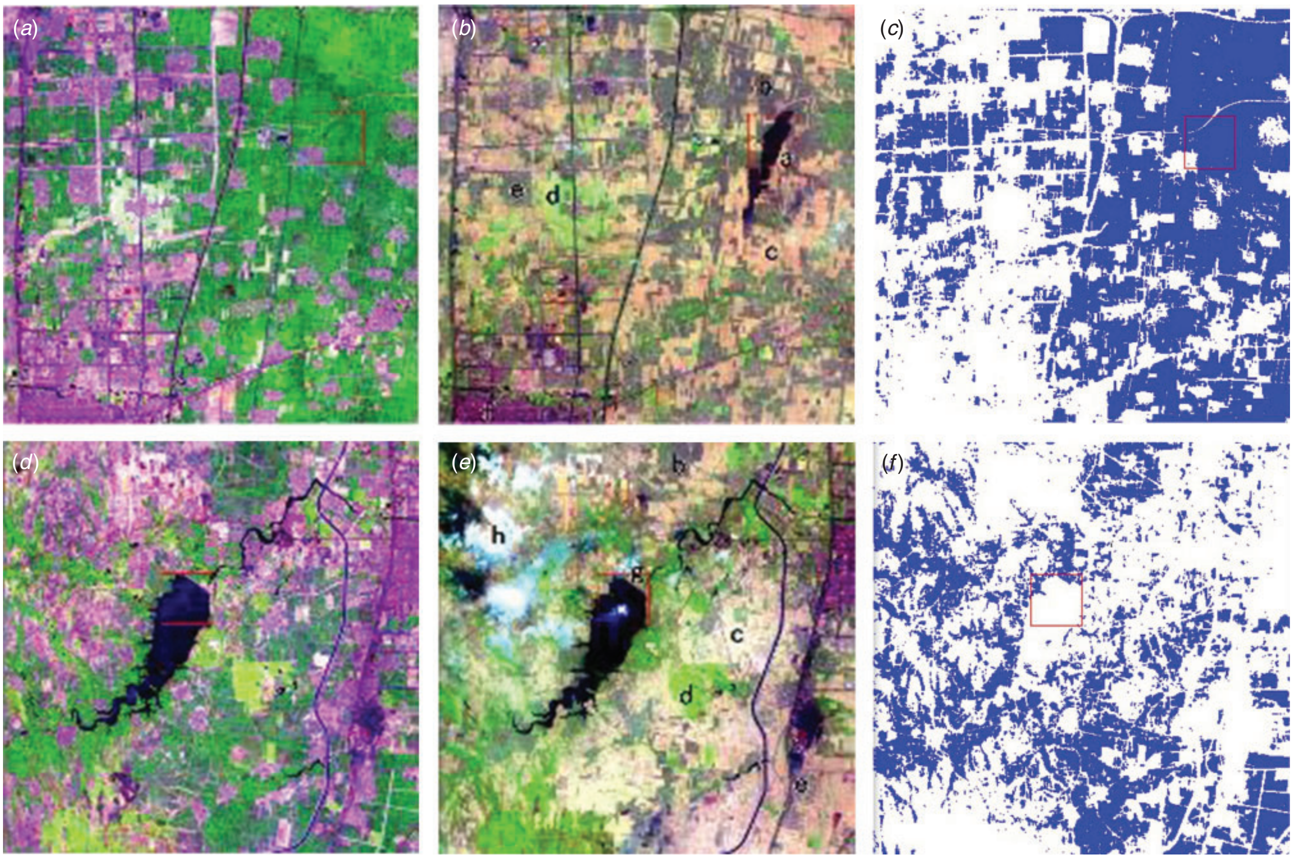

Fig. 8. Estimation of the area of mature winter wheat according to the VDI model. (*a*), (*b*), (*d*), and (*e*) were derived from Landsat 8 bands 6 (short-wave infrared (SWIR) 1), 5 (near-infrared (NIR)) and 4 (red) on Julian days 145 and 161. In Fig. 8, (a) is the burned area, (b) and (e) are stubble, and (c) is mature winter wheat. In Fig. 8*b*, *e*, the letter 'a' stands for the underlying surface of the city and town, 'b' and 'e' for stubble, 'd' for water body, 'g' for water body and 'h' for cloud; the blue part in (*c*) and (*f*) indicates mature winter wheat or stubble areas. The red square is generated by the image processing software, no meaning here.

Verification of the BSI model

The accuracy of the BSI model was verified through an intercomparison of 286 groups of Landsat-based BSI values with objects observed in high-resolution satellite imagery and field surveys. The accuracy assessment was performed within a short period of time after Landsat data acquisition. The validated burned area, roads and crop residue were obtained by field surveys and high-resolution remote sensing images (GF-1). The specific features corresponding to each class were digitised in the high-resolution images. The digitised features representing burned area, crop residue and roads were then used to produce a random stratified point sample for each class. Finally, this random sample of points was used as the ground truth for accuracy assessment of the Landsat-based classification. The false-positive, false-negative, missing alarm and false alarm (Table 5) rates were found to be acceptable according to evaluation of the target detection accuracy (Burke *et al.* 1988; Lienhart and Maydt 2002; Dumitrescu *et al.* 2003; Tyre *et al.* 2003).

Compared with other models, such as SAVI, the Char Soil Index (CSI) and BAI, the new method presented herein is clearly more effective for estimating burn scar areas.

Based on the BSI data in Fig. 9, a number of conclusions can be drawn. (1) The BSI model can estimate burned areas, such as in Fig. 9*c*, but shadows from clouds may result in misidentification (as seen in Fig. 9*f*) due to spectral differences between shallow cloud, smoke and burned areas. (2) Burned areas differed markedly in shape and size (Fig. 10). Large areas represent severe wildfires in mature winter wheat or stubble areas; within these areas, some of the fires were natural wildfires, whereas others were caused by straw burning. (3) A large number of burned areas were apparent in the images, indicating that agricultural

Table 5. Precision analysis of burned areas based on the Burn Scar Index (BSI) model

Abbreviations: SAVI, Soil Adjusted Vegetation Index; CSI, Char Soil Index; BAI, Burned Area Index; NBR, Normalized Burned Ratio; VDI, Vegetation Difference Index; BSI, Burn Scar Index

Model	False positive (FP)	False negative (FN)	Missing alarm rate (MAR)	False alarm rate (FAR)
VDI and BSI	28	49	0.098	0.160
SAVI	77	73	0.269	0.259
CSI	68	57	0.238	0.192
BAI	51	61	0.178	0.206
NBR	45	69	0.157	0.226

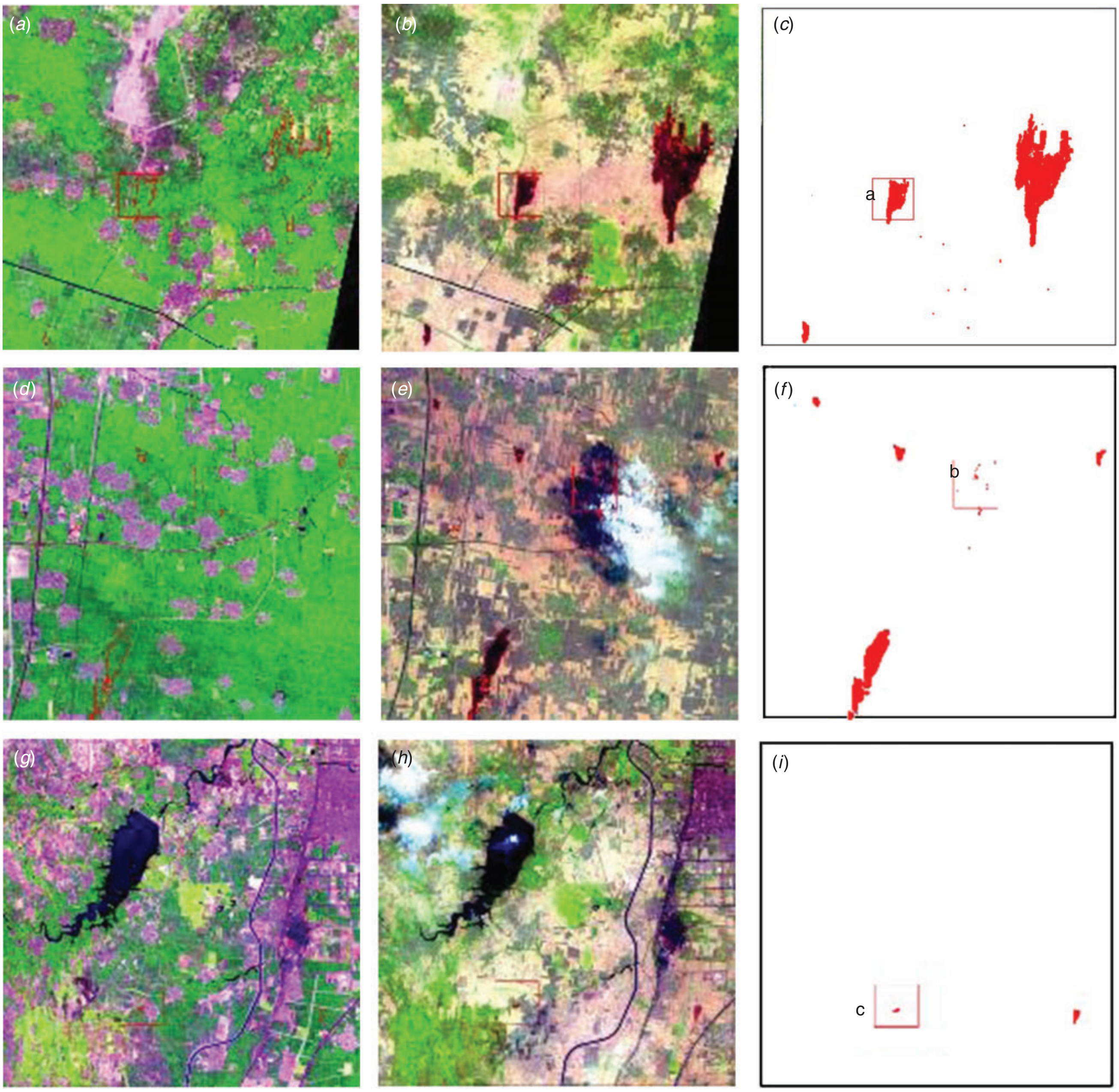

Fig. 9. Burned area estimates for different underlying surfaces (the letter 'a' and the other large red patches in (*c*) indicate areas burned by wildfires; the letter 'b' in (*f*) denotes cloud shadows, whereas 'c' in (*i*) indicates smoke from straw burning).

wildfires generally occur during the winter wheat harvesting season, and these fires may cause air pollution and grain loss.

Conclusions

To summarise, the following conclusions can be drawn. (1) Accurate identification of a crop planting area requires highly precise information on burned areas. During the harvest period, wildfires are often caused by prescribed fires that were set to burn crop straw or stubble. These wildfires are a direct cause of air pollution and grain loss, especially in north and north-east China (Shi *et al.* 2014; Long *et al.* 2016). The occurrence of wildfires is related to local climatic conditions and land-management practices. Therefore, local fire management personnel need to monitor both prescribed fires and areas affected by wildfires. (2) The VDI model may effectively simplify background information during monitoring of burned areas. Using to differences between the growth curves of crop areas and sources of background information, the VDI model was developed, which can be used to effectively estimate mature crop areas in regions where wildfires may occur. Through the use of the VDI model, certain types of background information, such as the locations of water bodies, grasslands and roads can be filtered out, with the result that the BSI model

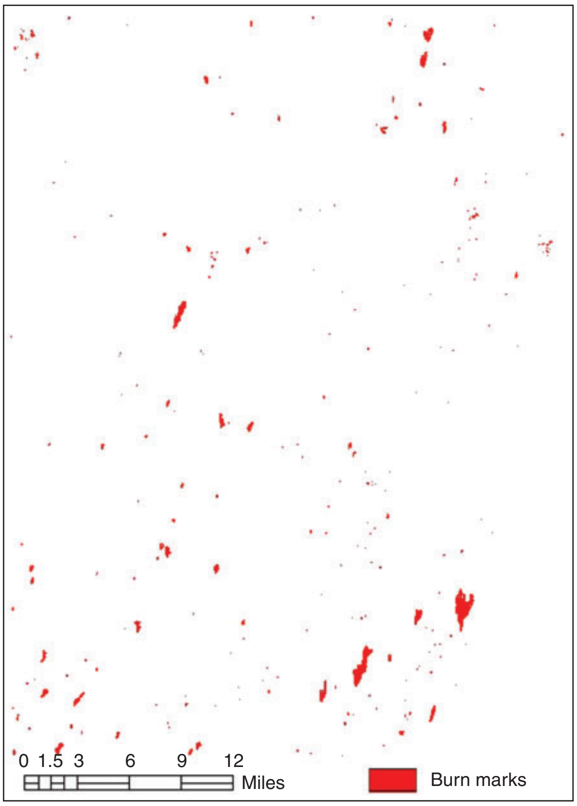

Fig. 10. Information extracted from the study area using the BSI model.

may be more effective for estimating burned areas. (3) The simulations and experiments conducted during this study showed that the BSI model was moderately reliable in determining crop areas. The parameters used in the BSI model were applied to the winter wheat planting area in the Haihe River Basin. The results showed that the BSI model may be sufficiently precise for monitoring burned areas; the VDI model was also shown to be effective.

However, when a comprehensive analysis was performed using a combination of on-site investigation, simulation analysis and remote sensing mapping, it was evident that the VDI model was more suitable for monitoring early harvest crops. The early harvest crop areas showed a different trend in cover changes to those of forests and grasslands, and cities and towns during the harvest period. When the growth curve trend changes, the VDI model should be adjusted according to crop type. With the BSI model, it was also difficult to differentiate burned areas of mature crops from burned areas of stubble because of the complexity of the soil spectrum in of burned stubble areas.

Conflicts of interest

The authors declare they have no conflicts of interest.

Acknowledgements

Research grants from the National Science Foundation of China (Grant no.s 41371359, 41671362), the Fundamental Research Funds for the Central Universities (Grant no. 2017B05114) and the Major Special Project – the China High-Resolution Earth Observation System (30-Y30B13-9003-14/16) supported this research. The authors would like to thank the anonymous reviewers for their helpful and constructive feedback.

References

Andreae MO, Crutzen PJ (1997) Atmospheric aerosols: biogeochemical sources and role in atmospheric chemistry. *Science* **276**, 1052–1058. doi:10.1126/SCIENCE.276.5315.1052

Andreae MO, Merlet P (2001) Emission of trace gases and aerosols from biomass burning. *Global Biogeochemical Cycles* **15**, 955–966. doi:10.1029/2000GB001382

Araújo FMD, Ferreira LG (2015) Satellite-based automated burned area detection: a performance assessment of the MODIS MCD45A1 in the Brazilian savanna. *International Journal of Applied Earth Observation and Geoinformation* **36**, 94–102. doi:10.1016/J.JAG.2014.10.009

Bastarrika A, Chuvieco E, Pilar Martin M (2011) Mapping burned areas from Landsat TM/ETM plus data with a two-phase algorithm: balancing omission and commission errors. *Remote Sensing of Environment* **115**, 1003–1012. doi:10.1016/J.RSE.2010.12.005

Boschetti M, Stroppiana D, Brivio PA (2010) Mapping burned areas in a Mediterranean environment using soft integration of spectral indices from high-resolution satellite images. *Earth Interactions* **14**, 1–20. doi:10.1175/2010EI349.1

Boschetti L, Roy DP, Justice CO, Humber ML (2015) MODIS–Landsat fusion for large-area 30-m burned area mapping. *Remote Sensing of Environment* **161**, 27–42. doi:10.1016/J.RSE.2015.01.022

Burke DS, Brundage JF, Redfield RR, Damato JJ, Schable CA, Putman P, Visintine R, Kim HI (1988) Measurement of the false positive rate in a screening program for human immunodeficiency virus infections. *The New England Journal of Medicine* **319**, 961–964. doi:10.1056/NEJM198810133191501

Carlson TN, Ripley DA (1997) On the relation between NDVI, fractional vegetation cover, and leaf area index. *Remote Sensing of Environment* **62**, 241–252. doi:10.1016/S0034-4257(97)00104-1

Chen W, Tong DQ, Dan M, Zhang S, Zhang X, Pan Y (2017) Typical atmospheric haze during crop harvest season in north-eastern China: a case in the Changchun region. *Journal of Environmental Sciences* **54**, 101–113. doi:10.1016/J.JES.2016.03.031

Chuvieco E, Martin MP, Palacios A (2002) Assessment of different spectral indices in the red–near-infrared spectral domain for burned land discrimination. *International Journal of Remote Sensing* **23**, 5103–5110. doi:10.1080/01431160210153129

Chuvieco E, Englefield P, Trishchenko AP, Luo Y (2008) Generation of long time series of burn area maps of the boreal forest from NOAA-AVHRR composite data. *Remote Sensing of Environment* **112**, 2381–2396. doi:10.1016/J.RSE.2007.11.007

Domenikiotis C, Dalezios NR, Loukas A, Karteris M (2002) Agreement assessment of NOAA/AVHRR NDVI with Landsat TM NDVI for mapping burned forested areas. *International Journal of Remote Sensing* **23**, 4235–4246. doi:10.1080/01431160110107707

Dumitrescu S, Wu X, Wang Z (2003) Detection of LSB steganography via sample pair analysis. *IEEE Transactions on Signal Processing* **51**, 1995–2007. doi:10.1109/TSP.2003.812753

França D, Longo K, Rudorff B, Aguiar D, Freitas S, Stockler R, Pereira G (2014) Pre-harvest sugarcane burning emission inventories based on remote sensing data in the state of Sao Paulo, Brazil. *Atmospheric Environment* **99**, 446–456. doi:10.1016/J.ATMOSENV.2014.10.010

French NHF, Kasischke ES, Hall RJ, Murphy KA, Verbyla DL, Hoy EE, Allen JL (2008) Using Landsat data to assess fire and burn severity in the North American boreal forest region: an overview and summary of results. *International Journal of Wildland Fire* **17**, 443–462. doi:10.1071/WF08007

Hao WM, Larkin NK (2014) Wildland fire emissions, carbon, and climate: wildland fire detection and burned area in the United States. *Forest Ecology and Management* **317**, 20–25. doi:10.1016/J.FORECO.2013.09.029

Houghton R, Hackler J, Lawrence K (2000) Changes in terrestrial carbon storage in the United States. 2: The role of fire and fire management. *Global Ecology and Biogeography* **9**, 145–170. doi:10.1046/J.1365-2699.2000.00164.X

Hudak AT, Brockett BH (2004) Mapping fire scars in a southern African savannah using Landsat imagery. *International Journal of Remote Sensing* **25**, 3231–3243. doi:10.1080/0143116031000163266

Huete AR (1988) A soil-adjusted vegetation index (SAVI). *Remote Sensing of Environment* **25**, 295–309. doi:10.1016/0034-4257(88)90106-X

Huete A, Didan K, Miura T, Rodriguez EP, Gao X, Ferreira LG (2002) Overview of the radiometric and biophysical performance of the MODIS vegetation indices. *Remote Sensing of Environment* **83**, 195–213. doi:10.1016/S0034-4257(02)00096-2

Jia K, Liang S, Gu X, Baret F, Wei X, Wang X, Yao Y, Yang L, Li Y (2016) Fractional vegetation cover estimation algorithm for Chinese GF-1 wide field view data. *Remote Sensing of Environment* **177**, 184–191. doi:10.1016/J.RSE.2016.02.019

Key C, Benson N (2006) Landscape assessment: remote sensing of severity, the Normalized Burn Ratio and ground measure of severity, the Composite Burn Index. In 'FIREMON: fire effects monitoring and inventory system. RMRS-GTR-164-CD'. (Eds D Lutes, R Keane, J Caratti, C Key, N Benson, S Sutherland, L Gangi) pp. LA 1–51. (USDA Forest Service, Rocky Mountain Research Station: Ogden, UT, USA)

Kučera J, Yasuoka Y, Dye DG (2005) Creating a forest fire database for the Far East of Asia using NOAA/AVHRR observation. *International Journal of Remote Sensing* **26**, 2423–2439. doi:10.1080/01431160410001735085

Lasaponara R (2006) Estimating spectral separability of satellite derived parameters for burned areas mapping in the Calabria region by using SPOT-vegetation data. *Ecological Modelling* **196**, 265–270. doi:10.1016/J.ECOLMODEL.2006.02.025

Li J, Song Y, Mao Y, Mao Z, Wu Y, Li M, Huang X, He Q, Hu M (2014) Chemical characteristics and source apportionment of $PM_{2.5}$ during the harvest season in eastern China's agricultural regions. *Atmospheric Environment* **92**, 442–448. doi:10.1016/J.ATMOSENV.2014.04.058

Lienhart R, Maydt J (2002) An extended set of Haar-like features for rapid object detection. In 'Proceedings of the international conference on image processing (ICIP)', 22–25 September 2002, Rochester, NY, USA. Vol 1. pp. 900–903. (IEEE: USA)

Loboda T, O'Neal KJ, Csiszar I (2007) Regionally adaptable dNBR-based algorithm for burned area mapping from MODIS data. *Remote Sensing of Environment* **109**, 429–442. doi:10.1016/J.RSE.2007.01.017

Long X, Tie X, Cao J, Huang R, Feng T, Li N, Zhao S, Tian J, Li G, Zhang Q (2016) Impact of crop field burning and mountains on heavy haze in the North China Plain: a case study. *Atmospheric Chemistry and Physics* **16**, 9675–9691. doi:10.5194/ACP-16-9675-2016

Maingi JK, Henry MC (2007) Factors influencing wildfire occurrence and distribution in eastern Kentucky, USA. *International Journal of Wildland Fire* **16**, 23–33. doi:10.1071/WF06007

McCarty JL, Korontzi S, Justice CO, Loboda T (2009) The spatial and temporal distribution of crop residue burning in the contiguous United States. *The Science of the Total Environment* **407**, 5701–5712. doi:10.1016/J.SCITOTENV.2009.07.009

Mitri GH, Gitas IZ (2004) A semi-automated object-oriented model for burned area mapping in the Mediterranean region using Landsat-TM imagery. *International Journal of Wildland Fire* **13**, 367–376. doi:10.1071/WF03079

Palandjian D, Gitas IZ, Wright R (2009) Burned area mapping and post-fire impact assessment in the Kassandra Peninsula (Greece) using Landsat TM and Quickbird data. *Geocarto International* **24**, 193–205. doi:10.1080/10106040802488542

Parker BM, Lewis T, Srivastava SK (2015) Estimation and evaluation of multidecadal fire severity patterns using Landsat sensors. *Remote Sensing of Environment* **170**, 340–349. doi:10.1016/J.RSE.2015.09.014

Pinty B, Verstraete M (1992) GEMI: a non-linear index to monitor global vegetation from satellites. *Plant Ecology* **101**, 15–20. doi:10.1007/BF00031911

Qi J, Chehbouni A, Huete A, Kerr Y, Sorooshian S (1994) A modified soil adjusted vegetation index. *Remote Sensing of Environment* **48**, 119–126. doi:10.1016/0034-4257(94)90134-1

Shi T, Liu Y, Zhang L, Hao L, Gao Z (2014) Burning in agricultural landscapes: an emerging natural and human issue in China. *Landscape Ecology* **29**, 1785–1798. doi:10.1007/S10980-014-0060-9

Smith AMS, Drake NA, Wooster MJ, Hudak AT, Holden ZA, Gibbons CJ (2007) Production of Landsat ETM plus reference imagery of burned areas within southern African savannahs: comparison of methods and application to MODIS. *International Journal of Remote Sensing* **28**, 2753–2775. doi:10.1080/01431160600954704

Conghe Song CH, Woodcock CE (2003) Monitoring forest succession with multitemporal Landsat images: factors of uncertainty. *IEEE Transactions on Geoscience and Remote Sensing* **41**, 2557–2567. doi:10.1109/TGRS.2003.818367

Stroppiana D, Boschetti M, Zaffaroni P, Brivio PA (2009) Analysis and interpretation of spectral indices for soft multicriteria burned-area mapping in Mediterranean regions. *IEEE Geoscience and Remote Sensing Letters* **6**, 499–503. doi:10.1109/LGRS.2009.2020067

Trigg S, Flasse S (2001) An evaluation of different bispectral spaces for discriminating burned shrub-savannah. *International Journal of Remote Sensing* **22**, 2641–2647. doi:10.1080/01431160110053185

Tyre AJ, Tenhumberg B, Field SA, Niejalke D, Parris K, Possingham HP (2003) Improving precision and reducing bias in biological surveys: estimating false-negative error rates. *Ecological Applications* **13**, 1790–1801. doi:10.1890/02-5078

Vadrevu K, Lasko K (2015) Fire regimes and potential bioenergy loss from agricultural lands in the Indo-Gangetic Plains. *Journal of Environmental Management* **148**, 10–20. doi:10.1016/J.JENVMAN.2013.12.026

Veraverbeke S, Verstraeten WW, Lhermitte S, Goossens R (2010*a*) Evaluating Landsat Thematic Mapper spectral indices for estimating burn severity of the 2007 Peloponnese wildfires in Greece. *International Journal of Wildland Fire* **19**, 558–569. doi:10.1071/WF09069

Veraverbeke S, Verstraeten WW, Lhermitte S, Goossens R (2010*b*) Illumination effects on the differenced Normalized Burn Ratio's optimality for assessing fire severity. *International Journal of Applied Earth Observation and Geoinformation* **12**, 60–70. doi:10.1016/J.JAG.2009.10.004

Veraverbeke S, Harris S, Hook S (2011*a*) Evaluating spectral indices for burned area discrimination using MODIS/ASTER (MASTER) airborne simulator data. *Remote Sensing of Environment* **115**, 2702–2709. doi:10.1016/J.RSE.2011.06.010

Veraverbeke S, Lhermitte S, Verstraeten WW, Goossens R (2011*b*) A time-integrated MODIS burn severity assessment using the multitemporal Differenced Normalized Burn Ratio (dNBR(MT)). *International Journal of Applied Earth Observation and Geoinformation* **13**, 52–58. doi:10.1016/J.JAG.2010.06.006

Verbyla DL, Kasischke ES, Hoy EE (2008) Seasonal and topographic effects on estimating fire severity from Landsat TM/ETM+ data. *International Journal of Wildland Fire* **17**, 527–534. doi:10.1071/WF08038

Wang S, Baig MHA, Zhang L, Jiang H, Ji Y, Zhao H, Tian J (2015) A simple Enhanced Water Index (EWI) for percent surface water estimation using Landsat data. *IEEE Journal of Selected Topics in Applied Earth Observations and Remote Sensing* **8**, 90–97. doi:10.1109/JSTARS.2014.2387196

Yang S, He H, Lu S, Chen D, Zhu J (2008) Quantification of crop residue burning in the field and its influence on ambient air quality in Suqian, China. *Atmospheric Environment* **42**, 1961–1969. doi:10.1016/J.ATMOSENV.2007.12.007